Computers and Mathematics with Applications 72 (2016) 1244–1262

Contents lists available at ScienceDirect

Computers and Mathematics with Applications

journal homepage: www.elsevier.com/locate/camwa

Unified graph-based multi-fluid model for gas–liquid pipeline flows

B. Krasnopolsky [a,b,*], A. Starostin [c], A.A. Osiptsov [b]

[a] Institute of Mechanics, Lomonosov Moscow State University, Russia
[b] Schlumberger Moscow Research Center, Russia
[c] Schlumberger Abingdon Technology Center, United Kingdom

ARTICLE INFO

Article history:
Received 13 July 2015
Received in revised form 20 March 2016
Accepted 17 June 2016
Available online 21 July 2016

Keywords:
Multiphase flow
Multi-fluid model
Drift–flux model
SIMPLE
Pipeline flows
Tree-like graph

ABSTRACT

We present a novel model of transient multiphase flow for gas–liquid mixtures in long pipelines. The study develops a general flexible formulation of a one-dimensional flow for complex multiphase mixtures in the presence of slip and mass exchange. Multi-fluid and drift–flux approaches are combined. The multi-fluid model governs the momentum balance for the fluids, and drift–flux correlations are used for modelling of the slip between individual components. A tree-like graph is introduced to describe the hierarchy of fluids and components within the mixture. The numerical implementation for an arbitrary number of components is based on the extension of the Semi-Implicit Method for Pressure-Linked Equations. Imbalances of equations are selected as criteria for iteration convergence. Specific corrections are discussed, including those proposed for the equilibrium gas-release model.

1. Introduction

Transient multiphase flows in circular pipes are encountered in various industrial applications, including hydrocarbon production and transport, chemical engineering, nuclear energy, and biomechanics. The key motivation for this work comes from the oil and gas industry, where accurate and robust modelling of multiphase flows is required for the design, execution, and control of a number of technologies, including wellbore startup and cleanup after drilling. Commonly, the initial wellbore flow involves several fluids of different properties, such as mud, cushion, brine, reservoir oil, gas, and water, and possibly other liquids, which are left in the wellbore and near-wellbore zone after drilling and completion. The first priority for engineers is to make sure the wellbore is cleaned of non-reservoir liquids and a stable flow of hydrocarbons is established. To protect safety and environment, an accurate and predictive model is required to prevent undesired events such as unstable flow regimes or unexpected long slugs of non-hydrocarbon liquids (e.g., reservoir water), which may kill the flare during well testing on an offshore rig and result in a serious environmental accident. Effective management of multiphase pipeline flows in industrial applications requires corresponding software based on fast and reliable physical models and numerical methods. They typically operate with one dimensional models, utilizing asymptotic long-channel approximation based on the large aspect ratio of the pipe. Derivation of these models and governing equations from the first principles of fluid mechanics with cross-section averaging procedure can be found in [1,2].

There are two most widely-accepted approaches to continuum modelling for complex multiphase mixtures in one-dimensional approximation: the "simplified" drift–flux model [3–5] and the "full" multi-fluid model [6–10]. The drift–flux

* Corresponding author at: Institute of Mechanics, Lomonosov Moscow State University, Russia.
E-mail addresses: krasnopolsky@imec.msu.ru (B. Krasnopolsky), AStarostin@slb.com (A. Starostin), AOsiptsov@slb.com (A.A. Osiptsov).

http://dx.doi.org/10.1016/j.camwa.2016.06.020
0898-1221/

model is based on a single momentum conservation equation written for the mixture. The phase velocities are expressed explicitly by the algebraic formulae through the mixture velocity, weighted by a profile parameter, and a phase drift velocity.

In the drift–flux approach, the algebraic expressions for phase velocities follow from the corresponding momentum conservation laws. These expressions can be derived from an analytical solution of a particular flow structure under specific assumptions and then calibrated against the experimental data. The no-slip velocity condition between two chemically similar fluids is the most simple relationship commonly used to track miscible fluids as tracers in the liquid phase. Originally, the drift–flux model was formulated for gas–liquid flow, where liquid is a continuous phase and gas is dispersed in the form of bubbles. From the momentum conservation equation for the dispersed phase, it follows that under the balance of the gravity, Stokes, and Archimedes forces exerted on the bubble, the velocity of bubbles can be expressed analytically through the mixture velocity and the slip (drift) velocity [11]. In [12], the correlation for bubble velocity was proposed for freely rising bubbles. This correlation was used in [13] to study bubble column dynamics.

Whereas originally the drift–flux model was proposed for a specific bubbly gas–liquid flow regime, it was later extended to cover the entire range of flow regimes that may occur in a two-phase gas–liquid flow in an inclined pipe. A series of experimental studies propose the correlations between phase and mixture velocities over a wide range of flow rates. Drift–flux correlations for gas–liquid and oil–water slip and a two-stage approach to model three-phase gas–oil–water flows were proposed in [4].

The drift–flux model is applicable to a wide range of flow regimes with non-inertial interphase slip [11]. The variety of flow regimes in the multiphase pipe flows is a challenging issue, which complicates the numerical modelling. According to [14], it is possible to recognize different flow regimes for high-contrast density of fluids: annular, stratified smooth, rolling waves, dispersed flow, and slugging. The drift–flux model is not applicable to predict the stratified-wavy and hydrodynamic slugging flow regimes, yet it captures the terrain-induced slugging. The particular relationships of the drift–flux model cover restricted intervals of parameters: pipe inclination angle and diameter, surface tensions, temperatures, densities and other. The limits of applicability for some correlations are discussed in [15]. To model flows beyond these limits, the parameters of the corresponding relationships should be tuned against experimental data.

On the contrary, in the multi-fluid model, each phase is treated as a separate continuum described by a momentum equation. In [6,7,16], the multi-fluid model was developed and applied for cooling problems. Paper [17] considers the modelling of oil–water emulsion and gas mixture in application to hydrocarbon transportation. Three-fluid models are formulated, when it is necessary to consider several immiscible liquids or to take into account dispersed phases. In near-horizontal pipes the gas–oil–water mixture may flow in separate layers. It is found that oil–water slip is significant and can provoke transition from stratified smooth regime to slugging [18]. The authors also offer the criteria for identification of flow regime in gas–oil–water flows and choice of friction terms. In [17,19], a momentum equation for droplets is introduced, so the droplets are considered as a third phase. As a result, the precise prediction of the pressure drop and other properties of the annular flow regime becomes possible. In [9], the authors considered four continua: gas, liquid, droplets and bubbles. The model contains the most comprehensive experimentally-calibrated closure relations for friction and interphase mass exchange.

The first generation of closure correlations for multi-fluid models was related to the flow regimes [6,7,16,17], which were identified in experiments. Once the flow regime is identified, the correlations for friction forces can be specified. The flow patterns for hydrocarbons and air–water flows are constructed, for example, in [17,20]. In [21], the authors proposed the criteria of the transitions between flow regimes. The criteria are based on the stability analysis of two-phase flows and validated with the patterns from [20].

Starting from [22], the next generation of multi-fluid models is constructed to be flow-regime independent. The following extension of the model in [9] introduces bubbles and droplets to predict the transitions from slugging to dispersed flow or annular flow. The model covers the transitions between all flow regimes.

To our knowledge, the most complex formulation of the multi-fluid model is realized for three fluids (gas, oil, and water) and an arbitrary number of components in the dynamic pipeline flow simulator OLGA [17]. In [9], the two-fluid model is proposed in a regime-independent formulation for four fields (continuous and dispersed gas and liquid). In applications, however, the number of fluids may significantly exceed three. Besides, each fluid may be present in the form of a continuous layer and dispersed droplets or bubbles. The model needs closure relations for friction with the walls and between layers and for interphase mass exchange. Hyperbolicity analysis of the resulting equations is important to ensure well-posedness of the initial–boundary value problem and stability of its numerical solution.

In this work, we propose a model that covers an arbitrary number of phases and is based on the combination of the multi-fluid and the drift–flux approaches. We will use a tree-like graph representation for the complex structure of the mixture. A SIMPLE-like iterative algorithm is adopted to solve the governing equations. The numerical method operates with the model graph, hence it is possible to simulate mixture of any complexity.

The outline of the paper is as follows. Section 2 describes the unified mathematical model for multiphase flow based on a tree-like graph and examples of the graphs for the well-known models presented in the literature. Section 3 provides examples of closures for the mathematical model, typical for the flow of gas–oil–water mixtures in oil and gas applications. Section 4 presents the numerical method based on the SIMPLE-like approach. The section with validation cases follows.

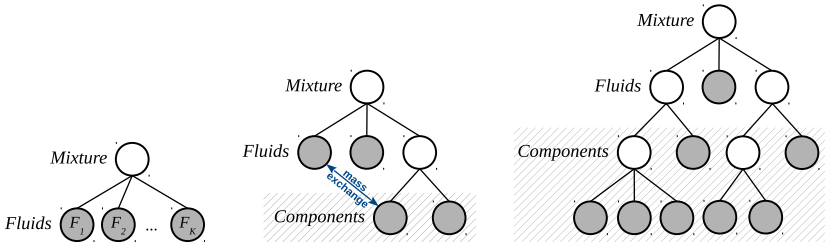

(a) K-fluid model: $S = K + 1, N = K, L = 1$.
(b) 3-fluid 4-phase model: $S = 6, K = 3, N = 4, L = 2$.
(c) 3-fluid 8-phase model: $S = 13, K = 3, N = 8, L = 5$.

Fig. 1. Tree-like graphs for various multiphase models. Terminal vertices are marked grey.

2. 1D flow regime-independent multiphase model

Let us first agree on the terminology which will be used throughout this paper. In the multi-fluid approach, by a fluid we will understand a mixture that is described by a separate momentum conservation equation in the model. The fluid is a mixture of components, which may belong to different phases. We will understand the phase in the sense of a phase state. We will consider three different phase states: solid, liquid and gas.

We consider a transient isothermal multiphase flow in a pipe of an arbitrary inclination, from horizontal to vertical. A mixture contains several immiscible compressible phases, such as gases and liquids. Each phase may be present in a continuous or a dispersed form (e.g., gas layer or bubbles, liquid layer or droplets).

2.1. Graph-based model formulation

The general 1D-model for several interpenetrating continua is formulated by using the cross-section averaged equations. The flow of K fluids is described within the multi-fluid formulation, where the motion of the fluids is governed by mass- and momentum-conservation laws. The mass balance equations for the fluids are written as

$$\frac{\partial \alpha_k \rho_k A}{\partial t} + \frac{\partial \alpha_k \rho_k u_k A}{\partial x} = J_k. \tag{1}$$

The momentum equations for the fluids are written in the form:

$$\frac{\partial \alpha_k \rho_k u_k A}{\partial t} + \frac{\partial \alpha_k \rho_k u_k^2 A}{\partial x} = -\alpha_k A \frac{\partial p}{\partial x} + F_k A - \Phi_k + I_k. \tag{2}$$

Here, A is the pipe cross-section. The unknown variables are pressure p, holdups α_k, and velocities u_k. The pressure p is the cross-section averaged thermodynamic pressure, which is equal in all phases. Densities ρ_k are specified as functions of pressure p. Mass exchange J_k includes inflow and mass exchange between the fluids. I_k is the momentum exchange due to mass exchange J_k. F_k is bulk force, and Φ_k is the friction force.

Mixture properties, such as holdup and average density and velocity, can be found using the following relations:

$$\alpha_M = \sum_{k=1}^{K} \alpha_k, \tag{3}$$

$$\alpha_M \rho_M = \sum_{k=1}^{K} \alpha_k \rho_k, \tag{4}$$

$$\alpha_M \rho_M u_M = \sum_{k=1}^{K} \alpha_k \rho_k u_k. \tag{5}$$

To close the system of governing equations (1)–(5), the holdup constraint should be taken into account:

$$\alpha_M = 1 \tag{6}$$

and equations of state should be specified:

$$\rho_k = \rho_k(p). \tag{7}$$

A multi-fluid model of K fluids (1)–(7) can be represented as a simple tree-like graph with a single root and K child vertices (Fig. 1(a)). The mixture is associated with the root vertex, while the child vertices correspond to the fluids. Thus,

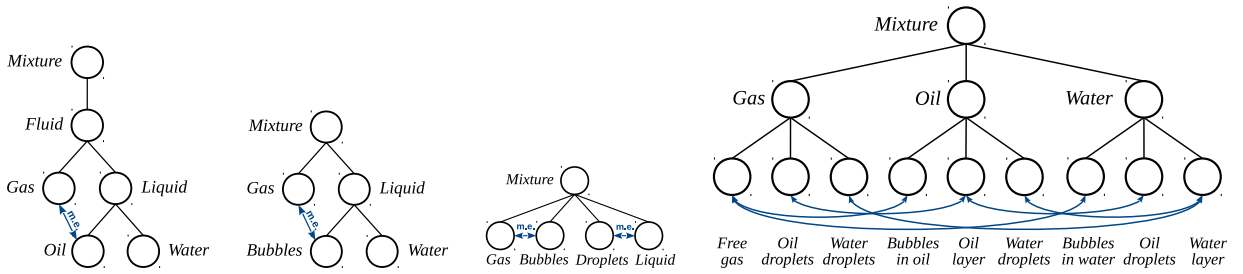

(a) Single-fluid wellbore flow model, [23].

(b) Two-fluid gas–liquid flow model, [24].

(c) Four-fluid gas–liquid flow model, [9].

(d) Pipe-transport flow model, [25].

Fig. 2. Tree-like graphs for familiar multiphase models, considered in publications.

the mass balance equations (1), momentum equations (2) and equations of state (7) are written for each terminal node of this tree. Edges of the tree represent the relations between holdups, densities, and velocities of the mixture and its components, which are described by relations (3)–(5). The model (1)–(7) includes $3S + 1$ unknown variables and equations, where $S = K + 1$ is the number of graph vertices.

Formally, the multi-fluid model can be formulated for an arbitrary number of fluids. In practice, however, the real number of fluids in the computational codes does not exceed three (see [17]). The reason for this limitation is the absence of complex closures for friction terms Φ_k in (2). These terms must include the contributions from each of the fluids that might require additional theory and experiments.

Alternatively, to-date, the correlations for the slip between various liquids and gases are well studied and one can choose to involve the slip correlations between some of the phases instead of the friction closures. This can be done with the help of the combination of the multi-fluid and drift–flux approaches on different levels of the graph-based model. Let us assume the fluid is also a mixture of several components. Components are compressible, may exchange mass and have different velocities. Interaction between the components can be described by drift–flux relations. The slip velocity is governed by the correlation as follows:

$$u_{c_1} - u_{c_2} = v_{c_1 c_2}(p, \alpha_{c_1}, \alpha_{c_2}, u_m); \tag{8}$$

here indices c_1 and c_2 enumerate the components inside the fluid m. This condition is supplemented by the mass balance equation (1), formulated for every terminal vertex of the tree. Taking into account relations (3)–(5), one can find the velocity for each of the components.

This extension of the multi-fluid model can be also represented on a tree-like graph. If one assumes the fluid consists of several components, the graph has an additional level. The vertex, corresponding to the composite fluid, has a set of child vertices, equal to the number of fluid components. An example of the model with three fluids and one of them with two components is presented in Fig. 1(b). The edges between the fluid and components specify relations between the holdups, densities and velocities (3)–(5), which are the same as in the case of the classical multi-fluid model. Vertices of the third level, corresponding to fluid components, are associated with mass balance equations (1), equations of state (7) and velocity slip relations (8).

The model can be extended to the case of composite components, which will require introducing an additional level on the graph (Fig. 1(c)). The same relations are applicable for an additional graph level: Eqs. (1), (7), and (8) for terminal vertices of the graph and (3)–(5) for composite component and its subcomponents.

Hence, we extend the multi-fluid model (1)–(8) for the general case of an arbitrary number of phases. Prior to mathematical formulation, we build a tree-like graph for a mixture. Let us define S as the total number of graph vertices, K as the number of vertices on the second level, corresponding to the number of fluids in the mixture, N as the number of terminal nodes, which is equal to the number of physical phases, and L as the number of non-terminal vertices. The model consists of one holdup constraint (6) and L holdup constraints (3), N mass balance equations (1), L average density relations (4), N equations of state (7), K momentum equations (2), L velocity relations (5) and $S - L - K$ slip velocity correlations (8). The total number of equations is $3S + 1$, that is equal to the number of unknown variables.

2.2. Examples of graphs constructed for the familiar models

Looking back at the publications on multiphase modelling we can reconstruct graphs for the mixtures. A single-fluid drift–flux model for multiphase wellbore flow is proposed in [23]. It covers gas–oil–water flows. The authors recognize gas and liquid as components of the first level (see Fig. 2(a)). The liquid is a composite component containing live oil and water.

In [24], the two-fluid model with bubble engagement and release is adjusted for slug capturing of multi-fluid modelling. The bubbles are fixed in liquid. There is a mass exchange between gas and bubbles as one of the components of the liquid. The corresponding graph for the model is shown in Fig. 2(b). In [9], the bubbles and droplets are considered as fluids to cover all flow regimes. There are mass exchanges in pairs gas–bubbles and droplets–liquid pairs. The graph for the model

formulation is shown in Fig. 2(c). However, the authors consider simulation cases in the simplified approach with algebraic equations instead of momentum equations for dispersed phases.

In [17] the momentum equation describes gas with droplets, while the droplet velocity depends on the flow parameters. Hence the gas with droplets is a single fluid with two components and a drift–flux relation between them. The extended variant of the model developed from [17] turned to the commercial simulator [25], where mixture can be described by three fluids and nine components (see Fig. 2(d)). The components of the same fluids slip between each other. The components of the same composition exchange masses between each other.

3. Closures for the physical interaction between the phases

To close the mathematical model (1)–(8), a set of relations, such as mass exchange J_k, momentum exchange I_k, velocity slip relations v_{ij}, frictions Φ_k and bulk forces F_k should be specified. This section contains typical examples of the closures used in our simulations.

3.1. Friction and bulk forces

For each fluid, the bulk forces include gravity force term, level gradient term, and the term with interfacial pressure:

$$F_k = -\alpha_k \rho_k g \left(\sin\beta + \cos\beta \frac{\partial H_L}{\partial x} \right) - P_I \frac{\partial \alpha_k}{\partial x}. \tag{9}$$

Here β is the inclination angle of the pipe (counter clockwise from the horizontal), g is gravity, H_L is height of the stratified liquid layer, P_I is the interfacial pressure. In order to describe the stratified flow regime, there is a hydrostatic term with the liquid level gradient. This term takes into account the hydrostatic pressure distribution in the pipe cross-section and renders a precise pressure distribution in the case of no motion in the pipe. Inclusion of this term yields conditional hyperbolicity of the model. In order to make the two-fluid model unconditionally hyperbolic, a synthetic term with interfacial pressure P_I is introduced (see also [7]). The specific form of this term is discussed in Appendix A.

For two-phase gas–liquid flows, the following expressions for the friction of the pipe walls and interphase friction are considered:

$$\Phi_G = \frac{\rho_G u_G |u_G|}{2} f_G S_G + \frac{\rho_G (u_G - u_L)|u_G - u_L|}{2} f_I S_I, \tag{10}$$

$$\Phi_L = \frac{\rho_L u_L |u_L|}{2} f_L S_L - \frac{\rho_G (u_G - u_L)|u_G - u_L|}{2} f_I S_I. \tag{11}$$

Here f_I, f_G, f_L are friction coefficients, and S_I, S_G, S_L are contact lengths. The Table B.4 in Appendix B contains friction coefficients and geometrical properties for various gas–liquid flow regimes. The second term in (10) and (11) evaluates friction between two fluids. For the interpenetrating continua the forces usually depend on the inertia of both continua, so the density difference is reasonable for scaling [2,26]. Though under the assumption of layered flows (stratified or annular) as there is no penetration of the fluids, the scaling is different. In experiments of [27], the friction factors were measured and their scales contain phase densities only.

It should be noted that momentum equation (2) with frictions (10) and (11) may degenerate in case of vanishing the fluid. This is a well known issue of the multi-fluid model, and it could lead to some difficulties in numerical modelling of slug flow regime. While this issue is not discussed in the paper in detail and is a focus of the further work, we would refer the readers to several publications discussing this issue and the ways to overcome it (see [7,22,28–30]). Formally, these options are consistent with the proposed unified graph-based model and could be applied for slug modelling.

3.2. Drift–flux model

The drift–flux model comprises the closure relations for slip velocity (8). It states the slip velocity between two components. The components form a fluid or a composite component with index m. Distinguishing light and heavy components with L and H indices correspondingly, the drift–flux correlation can be written in the form [31,4]:

$$u_L = C_0 v_m + V_D, \tag{12}$$

where C_0 is the profile parameter, v_m is volume velocity of the mixture m and V_D is the drift velocity. Generally, C_0 and V_D parameters may be derived under certain assumptions from the analytical models or obtained from the experimental data. The form of these expressions may vary depending on the physical process, specific components, pipe inclination angles, etc. The profile parameter recognizes the position of the phases in the pipe section. Normally C_0 varies from 1.0 to 1.2. The drift velocity is proportional to Stokes velocity with a coefficient varying from 0 to 2. The oil–water correlations used in this paper, were proposed in [31] as a result of processing the experimental data obtained for inclined and vertical pipes. These correlations are summarized in Table B.5 of Appendix B.

The correlation (12) is formulated via the volume velocity, while the presented model operates with mass velocity formulation. Using the volume velocity definition $\alpha_m v_m = \alpha_L u_L + \alpha_H u_H$ and taking into account conditions (3)–(5) one can obtain the expression for velocity slip (8) in the form:

$$u_L - u_H = \frac{\alpha_m^2 \rho_m \left(u_m(C_0 - 1) + V_D\right)}{\alpha_H \left(\alpha_m \rho_H - C_0 \alpha_L \left(\rho_H - \rho_L\right)\right)}. \tag{13}$$

Alternatively, the velocities for light and heavy components can be expressed in terms of mass mixture velocity:

$$u_L = C_L u_m + \frac{b_D}{\alpha_L \rho_L} V_D, \tag{14}$$

$$u_H = C_H u_m - \frac{b_D}{\alpha_H \rho_H} V_D, \tag{15}$$

where:

$$C_L = \frac{C_0 \alpha_m \rho_m}{C}, \tag{16}$$

$$C_H = \frac{(\alpha_m - C_0 \alpha_L)\alpha_m \rho_m}{\alpha_H C}, \tag{17}$$

$$b_D = \frac{\alpha_L \alpha_m \rho_L \rho_H}{C}, \tag{18}$$

$$C = \alpha_m \rho_H - C_0 \alpha_L (\rho_H - \rho_L). \tag{19}$$

Eqs. (14)–(15) provide explicit relations for the components velocities through the velocity of the mixture and this form of expressions will be used in the computations. In the limiting case of no slip between the components (i.e. $C_0 = 1$ and $V_D = 0$ in (12)), Eqs. (14)–(15) are reduced to the form $u_L = u_m$ and $u_H = u_m$, respectively.

The drift–flux approach is applicable for velocity slip between two components. Whenever there are more than two components that slip within a single fluid, the components can be split recursively by pairs, as it is proposed in [4]. The corresponding graph for the fluid with components, resolved by drift–flux relations, will have binary tree structure for these levels.

3.3. Gas-release model

Natural reservoirs contain live oil that releases gas under decompression. For modelling of upstream flows, two components should be present: a natural gas and an oil. To evaluate gas release, it is convenient to measure a number of values as functions of pressure. Among them are volume formation factors for oil and gas, $B_O(p)$ and $B_G(p)$, and gas–oil ratio, $R_S(p)$. The volume formation factor characterizes the ratio of the volume of the phase to the volume at standard pressure. The gas–oil ratio is the ratio of the volume of gas, that comes out of oil, to the volume of live oil, both measured at standard conditions. Being put in the relationships, the functions constitute black oil model (e.g., [32]):

$$\rho_N = \frac{\rho_G^{std}}{B_G}, \tag{20}$$

$$\rho_O = \frac{\rho_O^{std}}{B_O} + \frac{\rho_G^{std} R_S}{B_O}. \tag{21}$$

Here ρ_O^{std} and ρ_G^{std} are oil and gas densities at the standard conditions. These equations can be represented in the form:

$$\rho_i = \rho_{i1} + \rho_{i2}, \tag{22}$$

where ρ_{i1} corresponds to the first term of (20) and (21), while ρ_{i2} corresponds to the dissolved gas term in (21). The second term, ρ_{i2}, would be nonzero for the phases with dissolved gas (e.g., live oil phase and all the phases that correspond to the parent vertices of the model graph). In all other cases, ρ_{i2} is identically equal to zero. In the current work R_S was chosen as a piecewise linear function characterized by bubble point pressure P_S and maximum gas–oil ratio R_{S0}:

$$R_S(p) = \begin{cases} R_{S0}\, p/P_S, & p < P_S; \\ R_{S0}, & p \geq P_S. \end{cases} \tag{23}$$

The following mass conservation equations are stated for bulk oil and live oil with gas:

$$\frac{\partial \alpha_O \rho_{O1} A}{\partial t} + \frac{\partial \alpha_O \rho_{O1} u_O A}{\partial x} = J_O, \tag{24}$$

$$\frac{\partial \left(\alpha_O \rho_O + \alpha_N \rho_N\right) A}{\partial t} + \frac{\partial \left(\alpha_O \rho_O u_O + \alpha_N \rho_N u_N\right) A}{\partial x} = J_O + J_N. \tag{25}$$

The mass balance equation[1] (25) can be reformulated in the form (1) for natural gas phase by the substitution of Eq. (24), with mass exchange-related inflow:

$$J_{GR} = -\frac{\partial \alpha_O \rho_{O2} A}{\partial t} - \frac{\partial \alpha_O \rho_{O2} u_O A}{\partial x}. \tag{26}$$

This form of mass balance equation with mass inflow (26) preserves the overall standard formulation for mass balance equations, which is crucial for implementation of unified computational procedure operating with model graphs. This inflow leads to an additional coupling between the mass balance equations, and some additional efforts must be taken for the numerical solution of these equations.

Black oil model specifies an equilibrium gas release (see Fig. 1(b)) and gas dissolution in case of negative J_{GR}. Though the dissolution may result in complete disappearance of gas, then the black oil model is no longer applicable. More complex compositional models and non-equilibrium gas release may be required to account for the deviations from black oil behaviour (see also [1,33]).

An averaged momentum exchange term is a product of mass exchange and interfacial velocity. As gas release happens at the bubble surface, the interfacial velocity is equal to the liquid velocity. Gas dissolution most likely takes place at the surface; due to surface complexity, the primary assumption about its velocity can be a mixture velocity. The momentum exchange term can be specified as:

$$I_{GR} = \max(0, J_{GR}) u_O + \min(0, J_{GR}) \frac{\alpha_O \rho_O u_O + \alpha_N \rho_N u_N}{\alpha_O \rho_O + \alpha_N \rho_N}. \tag{27}$$

The ratio of the mass exchange term to the mixture flow is evaluated like

$$\frac{J_{GR}}{\frac{\partial \alpha \rho A}{\partial x}} \approx \frac{\rho_G^{std}}{\rho_O^{std}} R_{S0}. \tag{28}$$

The ratio of the momentum exchange term to the mixture pressure gradient is expressed as

$$\frac{I_{GR}}{A \frac{\partial p}{\partial x}} \approx \frac{2\rho_G^{std}}{\rho_O^{std}} \frac{R_{S0}}{Eu}, \tag{29}$$

$$Eu = \frac{2\delta P}{\rho_O^{std} U^2}. \tag{30}$$

Here Eu is the Euler number calculated with typical pressure drop δP and typical velocity U. As $Eu \gg 1$ and $\rho_G^{std} R_S \approx \rho_O^{std}$, momentum exchange can be neglected, while the mass exchange has to be accounted for in most cases governed by the black-oil model.

The formulated gas-release and dissolution mass exchange model is an example of the mass transfer mechanism between the phases that may take place in pipe flows. However, to model various flows of complex mixtures the variety of processes with mass transfer between the dispersed and continuous phases, such as droplets atomization and deposition or gas–bubbles entrainment and disengagement, should be considered in general multi-phase flow simulators. While these mechanisms with corresponding specific correlations are not yet considered and validated in this study, it is expected that the proposed graph-based approach and the mathematical model could naturally be extended to simulate the flows with such phenomena. It can be done by the introduction of the vertices on the graph for dispersed and continuous phases, with corresponding mass exchange correlations (as it is done in [34], Fig. 2(d)). This is one of the questions to be dealt with in a future work.

4. Numerical method

A variety of numerical methods were developed for multiphase pipe flows, depending on the physical process of interest. Three main directions with their strengths and weaknesses are distinguished: explicit Godunov-type schemes, Semi-Implicit Methods for Pressure-Linked Equations (SIMPLE), and fully implicit Newton–Raphson-based iterative methods. The present paper is focused on the generalization for the second type, semi-implicit methods, to handle with graph-based model formulation.

The SIMPLE was initially developed for single-phase flows [35]. It belongs to the family of segregated methods, where each unknown variable is calculated from a corresponding equation separately from other variables (predictor stage). As the governing equations are non-linear and coupled, an iterative procedure on each time step might be needed to satisfy all the equations (corrector stage). A set of methods with different number of predictor and corrector stages and correction expressions has been developed to date. An overview of the most relevant modifications can be found, for example, in [36].

[1] In the presence of mass exchange due to gas release, the densities in mass balance equations (1) should be treated as ρ_{k1}, while the momentum equations (2) should be formulated for the full fluid densities ρ_k. Relations (4) are satisfied for both densities summands.

Two types of methods are distinguished depending on the principle of construction for correction equations. The first type of methods, Mass Conservation-Based Algorithms (MCBA), assumes the use of velocities and pressure corrections and formulation of pressure correction equation from the overall mass balance equation [37]. The holdups are not involved into the corrections and are calculated after the variables correction stage. The second family of the methods, Geometry Conservation-Based Algorithms (GCBA) [38], assumes involvement of velocities, pressure and holdups into the correction procedure. The pressure correction equation for GCBA is derived from the holdup constraint. An overview of the methods based on mass and geometry conservation principles can be found in [39,40] respectively.

Both mass and geometry conservation based algorithms can be adopted to handle the model graph representation. The main attention in the paper would be focused on the GCBA approach as it was found preferable for gas-release modelling. The generalization for MCBA methods family to handle with proposed graph-based model formulation can be found in Appendix C.

For the sake of simplicity the following presentation would be focused on the SIMPLEC algorithm, while the same reasoning can be applied for any method from the SIMPLE algorithms family.

4.1. Geometry conservation-based approach

Following GCBA, solution for the next time step begins with obtainment preliminary velocity fields u_k^* by solving momentum equations (2) for every fluid vertex on the graph. Having the velocities for the fluids, one can restore the preliminary velocities for the mixture and fluid components. The mixture velocity, moving upward over the graph, is calculated using the relation (5). The velocities of components are found by moving downwards over the graph using the transformed drift–flux relations (14) and (15).

Calculation of the preliminary holdups α_i^* starts from the solution of mass balance equations (1) for terminal vertices of the graph. Then, using the holdup constraints (3) and moving upward over the graph, the preliminary holdups for all non-terminal graph vertices can be restored. If the preliminary mixture holdup for the root vertex α_M^* is close enough to unity (6), the obtained velocity and holdup distributions satisfy the mass balance equations and do not need any correction on the iteration. Otherwise, the correction procedure should be applied.

The correction procedure is built on the following principle. All the variables are represented in the form of main (preliminary) values and their corrections:

$$p^{n+1} = p^* + p', \qquad \rho_i^{n+1} = \rho_i^* + \rho_i', \qquad \alpha_i^{n+1} = \alpha_i^* + \alpha_i', \qquad u_i^{n+1} = u_i^* + u_i'. \tag{31}$$

Substituting these expressions into (2) one can obtain fluid velocity correction expressions in the form:

$$u_k' = u_k'\left(p'\right). \tag{32}$$

Additionally, the velocity corrections for all the components should be introduced. Thanks to the linear dependence of drift–flux relations (14)–(15) on the mixture velocity, the corrections for the components velocities can be represented as

$$u_L' = C_L u_m', \tag{33}$$

$$u_H' = C_H u_m'. \tag{34}$$

The pressure correction equation in geometry conservation methods is constructed from the condition $\alpha_M^{n+1} = \alpha_M^* + \alpha_M' = 1$. Thus, α_M' should be expressed as a function of the pressure correction. On the basis of expressions (3), the correction for the mixture holdup is defined as a sum of holdup corrections of the mixture components. Propagating this statement downward over the graph, the mixture correction α_M' can be expressed as a sum of holdup corrections for all terminal nodes:

$$\alpha_M' = \sum_{i=1}^{N} \alpha_i' = 1 - \alpha_M^*. \tag{35}$$

To complete the procedure, the holdup correction expressions should be derived from the mass balance equations as a function of pressure correction:

$$\alpha_i' = \alpha_i'\left(\rho_i'\left(p'\right), u_i'\left(p'\right)\right). \tag{36}$$

Finally, the densities corrections for terminal vertices are derived from the equations of state (7):

$$\rho_i' = C_i^{\rho} p', \tag{37}$$

where $C_i^{\rho}(p) = \partial\rho_i/\partial p$ is the compressibility factor.

Having pressure correction distribution from the solution of (35), one can correct velocities and holdups. Velocity correction starts with the fluids and, using corrections (33)–(34), can be propagated for all the phases downward on the graph. Holdup correction is started from the terminal vertices and is propagated upward the graph. Phase density corrections

also start from the terminal vertices using equations of state (7) and new corrected pressure field. From the terminal vertices the information can be propagated upwards with new component holdups values.

To conclude, the geometry conservation algorithm for graph-based model to compute the next time step consists of seven steps:

1. Find preliminary velocity fields u_k^* for the fluid phases; calculate velocities for the components.
2. Solve mass balance equations for terminal vertices to obtain preliminary holdup values; restore values for all phases.
3. Check for equations imbalances; if they are lower than the limiting values than go to Step 7, else go to Step 4.
4. Solve pressure correction equation, find pressure correction p'.
5. Correct velocities, holdups, and pressure.
6. Update density fields using new pressure distribution.
7. Check convergence criteria; continue non-linear iterations from Step 1 if convergence is not reached.

4.2. Spatial and temporal discretization

This subsection contains the description of numerical methods applied in the research code. While the numerical methods used are rather basic, the goal is to demonstrate the applicability for the unified graph-based approach to model various flows with complex mixtures.

In the present work, a uniform staggered grid is used: $x_{j+1} = x_j + h$, $j = 0, \ldots, N-1$. The pipe boundaries match the cells faces: $x_0 = 0$, $x_N = X$. The velocities are defined at cell faces and denoted with integer indices, while the pressure, holdups, and densities are defined at cell centres and denoted with semi-integer indices. The spatial discretization is constructed using the finite volume method. The implicit first order time integration scheme for mass balance and momentum equations is applied. Convective terms of equations are approximated according to the first- or the second-order upwind difference schemes on 3- or 5-point stencils correspondingly.

For a time step τ, $t^{n+1} = t^n + \tau$, and grid spacing h, the following discretizations for Eqs. (2) and (1) are used correspondingly:

$$A_j \frac{\tilde{\alpha}_{k,j}\tilde{\rho}_{k,j}u^*_{k,j} - \alpha^n_{k,j}\rho^n_{k,j}u^n_{k,j}}{\tau} + \frac{\tilde{\alpha}_{k,j+1/2}\tilde{\rho}_{k,j+1/2}\tilde{u}_{k,j+1/2}A_{j+1/2}u^*_{k,j+1/2}}{h} - \frac{\tilde{\alpha}_{k,j-1/2}\tilde{\rho}_{k,j-1/2}\tilde{u}_{k,j-1/2}A_{j-1/2}u^*_{k,j-1/2}}{h} = -\tilde{\alpha}_{k,j}A_j\frac{p^*_{j+1/2} - p^*_{j-1/2}}{h} + \tilde{F}_{k,j}A_j - \Phi^*_{k,j} + \tilde{I}_{k,j}, \tag{38}$$

$$A_{j+1/2}\frac{\alpha^*_{i,j+1/2}\tilde{\rho}_{i,j+1/2} - \alpha^n_{i,j+1/2}\rho^n_{i,j+1/2}}{\tau} + \frac{\alpha^*_{i,j+1}\tilde{\rho}_{i,j+1}u^*_{i,j+1}A_{j+1} - \alpha^*_{i,j}\tilde{\rho}_{i,j}u^*_{i,j}A_j}{h} = J_{i,j+1/2}. \tag{39}$$

Here, the first index in expressions identifies the fluid, component or phase, and the second index corresponds to the cell number. The tilde denotes the variables and expressions taken from the previous non-linear iteration. The $u^*_{k,j}$ and $\alpha^*_{i,j+1/2}$ are the velocities and holdups from the current iteration to be found. The values $u^*_{k,j+1/2}$ and $\alpha^*_{i,j}$ at the faces of the corresponding control volumes are expressed with help of the first- or the second-order upwind difference scheme. All other variables, defined at cell centres, but used at cell faces, or vice versa, are linearly interpolated. The non-linear friction term Φ^*_k on the right-hand side of momentum equations (38) is linearized as

$$\Phi^*_{k,j} = \hat{\Phi}_{k,j}u^*_{k,j} + \tilde{\Phi}_{k,j}, \tag{40}$$

and included into implicit discretization. For the two-fluid gas–liquid frictions (10)–(11) the following approximation is used:

$$\Phi^*_{G,j} = \left(\frac{\tilde{\rho}_G|\tilde{u}_{G,j}|}{2}\tilde{f}_{G,j}\tilde{S}_{G,j} + \frac{\tilde{\rho}_{G,j}|\tilde{u}_{G,j} - \tilde{u}_{L,j}|}{2}\tilde{f}_{I,j}\tilde{S}_{I,j}\right)u^*_{G,j} - \frac{\tilde{\rho}_{G,j}\tilde{u}_{L,j}|\tilde{u}_{G,j} - \tilde{u}_{L,j}|}{2}\tilde{f}_{I,j}\tilde{S}_{I,j}, \tag{41}$$

$$\Phi^*_{L,j} = \left(\frac{\tilde{\rho}_L|\tilde{u}_{L,j}|}{2}\tilde{f}_{L,j}\tilde{S}_{L,j} + \frac{\tilde{\rho}_{G,j}|\tilde{u}_{G,j} - \tilde{u}_{L,j}|}{2}\tilde{f}_{I,j}\tilde{S}_{I,j}\right)u^*_{L,j} - \frac{\tilde{\rho}_{G,j}\tilde{u}_{G,j}|\tilde{u}_{G,j} - \tilde{u}_{L,j}|}{2}\tilde{f}_{I,j}\tilde{S}_{I,j}. \tag{42}$$

The exact form of corrections for velocities (32) and holdups (36) depends on the type of the computational grid, temporal and spatial discretization schemes and correction algorithms used (specific method from the SIMPLE algorithms family). For the SIMPLEC algorithm, based on (38), the velocity correction as a function of pressure correction can be represented as

$$u'_{k,j} = -\frac{\tau}{h}\gamma_{k,j}\left(p'_{j+1/2} - p'_{j-1/2}\right) \tag{43}$$

with

$$\gamma_{k,j} = \left(\tilde{\rho}_{k,j} + \frac{\tau\hat{\Phi}_{k,j}}{\tilde{\alpha}_{k,j}A_j} + \frac{\tilde{\alpha}_{k,j+1/2}\tilde{\rho}_{k,j+1/2}\tilde{u}_{k,j+1/2}A_{j+1/2}}{h\tilde{\alpha}_{k,j}A_j} - \frac{\tilde{\alpha}_{k,j-1/2}\tilde{\rho}_{k,j-1/2}\tilde{u}_{k,j-1/2}A_{j-1/2}}{h\tilde{\alpha}_{k,j}A_j}\right)^{-1}. \tag{44}$$

The coefficient γ_i for the fluid components is a multiplication of γ_k for the basic fluid and all the corresponding coefficients C_L or C_H on the graph path between the current and parent fluid vertices.

Preserving corrections for the density in the time derivative term and velocity corrections for the convective term in (1), the following expression can be constructed for holdups:

$$\alpha'_{i,j+1/2} = -\frac{\alpha^*_{i,j+1/2}}{\tilde{\rho}_{i,j+1/2}} C_i^{\rho} p'_{j+1/2} - \frac{\tau}{h} \frac{1}{A_{j+1/2}\tilde{\rho}_{i,j+1/2}} \left(\alpha^*_{i,j+1}\tilde{\rho}_{i,j+1}u'_{i,j+1}A_{j+1} - \alpha^*_{i,j}\tilde{\rho}_{i,j}u'_{i,j}A_j\right). \tag{45}$$

4.3. Gas-release model extension

The mass exchange flux (26) between the natural gas and live oil phases depends on the pressure, volume holdup, and velocity of the oil phase. This dependence leads to a strong coupling between the live oil and natural gas mass balance equations that may affect the global iterations convergence rate. As it was found during numerical experiments, an attempt to discretize the flux J_{GR}, using the values from the previous time step or even from the previous iteration at the current time step may fail the convergence of non-linear iterations.

The observed issue can be resolved for GCBA methods by involvement of the flux J_{GR} into the iterations and formulation of corrections for $J'_N = J'_{GR}$ as a function of pressure correction:

$$J'_{GR}(p') = J'_{GR}\left(\alpha'_O(p'), \rho'_{O2}(p'), u'_O(p')\right). \tag{46}$$

Thus, the holdup correction expression (45) for natural gas would have an additional term $J'_{N,j+1/2}\tau/(A_{j+1/2}\rho^*_{N1,j+1/2})$.

The correction expression for mass exchange flux J'_{GR} may be obtained by the same principle as for holdup correction and mass balance equation. In practice, however, even the simplest form

$$J'_{GR,j+1/2} = -\frac{\alpha^*_{O2,j+1/2}\rho'_{O2,j+1/2}A_{j+1/2}}{\tau}, \tag{47}$$

preserving correction for live oil density time derivative term only, was applicable for numerical modelling to provide acceptable convergence rate.

The proposed correction assumes the presence of additional terms for the holdup correction expressions. While the holdup corrections are used in geometry-based methods, the applicability of this approach is limited to the GCBA schemes only.

4.4. Convergence criteria

Various criteria can be chosen to monitor the convergence for non-linear iterations. Among the common variants are the absolute or relative norms for increments of physical variables (i.e. $\|f_i^{l+1} - f_i^l\| < \varepsilon_{tol}$ or $\|f_i^{l+1} - f_i^l\|/\|f_i^{l+1}\| < \varepsilon_{tol}$). Here l is the number of non-linear iteration and L_∞ can be used as a vector norm. This criteria means the maximum increment for solution vector after the non-linear iteration becomes smaller than the prescribed value. This condition, however, is necessary but not sufficient, as it generally does not guarantee that the obtained solution satisfies the discrete form of governing equations. The more strict condition is the equations imbalance criteria: the obtained solution after the non-linear iteration is substituted into the numerical approximation scheme and residuals for each of equations are considered. The convergence in terms of imbalances guarantees that the numerical solution approximates the governing equations with prescribed tolerances.

The impact of choice of the convergence criteria will be demonstrated for the holdup normalization technique with the MCBA scheme when the obtained solution satisfies the norm in terms of vector increment but not the equations imbalances.

5. Validation

This section considers simulation cases with interfacial waves, oil–water segregation, stabilization of gas–oil flow, and a flow of five-phase mixture in a wellbore. The mixtures in simulation cases are based on different graphs. The cases are ordered by graph complexity and validate the principal aspects of the model.

5.1. Interfacial waves

The model describes a well-known phenomena of interfacial waves growth in the near-horizontal pipe, produced by the Kelvin–Helmholtz instability mechanism. The problem considers air–water flow. Two-fluid model corresponds to the graph in Fig. 3(a). The pipe has inclination $\beta = -5^\circ$, diameter $D = 0.051$ m and length $L = 30$ m. The specified inlet holdups oscillate with time as $\alpha_k = \alpha_{k0} \pm 0.005 \sin(2\pi t/T)$, $T = 2$ s, $\alpha_{W0} = 0.5311$, $\alpha_{G0} = 0.4689$. The inlet velocities are constant

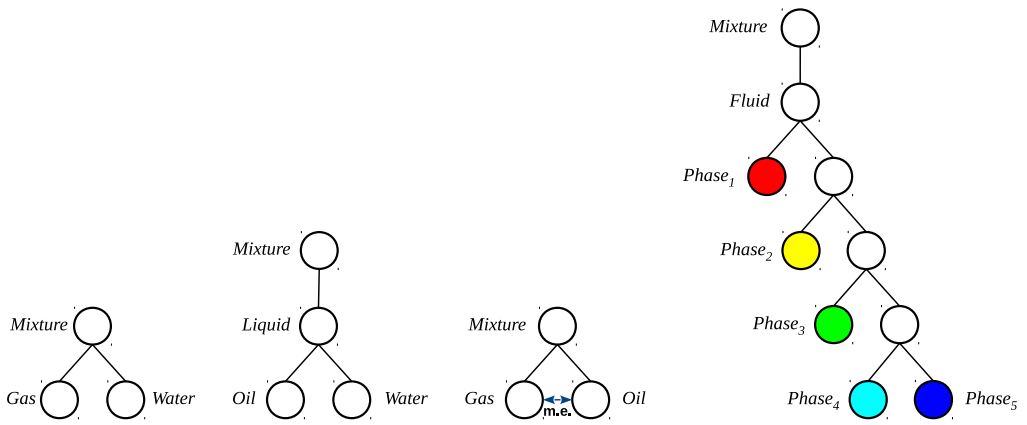

(a) Interfacial waves. (b) Oil–water segregation case. (c) Stabilization of gas–oil flow. (d) 5-phase mixture flow in a wellbore.

Fig. 3. Tree-like graphs for various test cases considered.

Table 1
Parameters of PVT tables for phases at reference pressure $P^{std} = 10^5$ Pa.

Fluid	Air/Gas	Oil	Water
Viscosity, $\mu \times 10^3$ (Pa s)	0.017	0.74	1
Reference density, ρ^{std} (kg/m^3)	1.22	800	1000
Gas–oil ratio, R_{S0}	0	800	0
Bubble pressure, $P_S \times 10^{-5}$ (Pa)	–	100	–
Volume formation factor, B	$\frac{P^{std}}{p}$	$\frac{1}{1+C^{\rho}(p-P^{std})}$	$\frac{1}{1+C^{\rho}(p-P^{std})}$
Compressibility, $C^{\rho} \times 10^5$ (Pa^{-1})	–	10^{-4}	10^{-4}

Table 2
Grid convergence for the two-phase interfacial waves test problem.

Grid size	2000	4000	8000	16 000	Theoretical
Wave length (m)	4.888	4.894	4.897	4.899	4.9
Amplification factor (m^{-1})	0.054	0.062	0.067	0.068	0.067

and defined as $u_k = q_{k0}/\alpha_{k0}$ with inlet rates $q_{G0} = q_{W0} = 1$ m/s. The pressure at the outlet of the pipe is constant and equal to 10^5 Pa. The densities and viscosities of the fluids are specified in Table 1.

The specified conditions correspond to the uniform solution by the steady state model. The stratified flow has a uniform initial distribution with holdups and velocities, corresponding to inlet values at time $t = 0$ s. However, the steady state flow is unstable and evolves to periodic behaviour. The inlet oscillations induce a growth of interfacial waves. Their amplitude and length correspond to the unstable mode. The mode is sustained by the inlet perturbation. The profiles of growing waves for different computational grids are shown in Fig. 4. Results demonstrate the grid convergence in terms of the wave length and the amplification factor, as shown in Table 2. For the extrapolated wave length $L = 4.9$ m, the analytical value for the amplification factor is obtained with help of linear stability theory. The properties of the waves in the unstable stratified flow are evaluated by the dispersion equation (see [21]). The good correspondence between the numerical and theoretical values is observed.

The MCBA and GCBA numerical schemes are compared in terms of cumulative number of non-linear iterations for simulation of a predefined time interval. For a grid with $N = 1000$ cells and constant time step $\tau = 10^{-2}$ s (which provides local Courant number $C \sim 1$) the time interval of 30 s is simulated. As a criteria of convergence for non-linear iterations, equations imbalances are monitored. Here, the maximum imbalance 10^{-4} is specified for the momentum and mass balance equations and 10^{-6} for the holdup constraint. These imbalance values guarantee that the observed solution matches between all the numerical schemes.

The number of non-linear iterations as a function of simulated time (time step number) is presented in Fig. 5. The option to drop one of the mass balance equations is investigated for MCBA. Both variants to drop air or water mass balance equations are considered. For the prescribed flow and set of parameters the MCBA scheme demonstrates almost linear dependence of the cumulative number of iterations on the simulation time, i.e., constant number of iterations per time step. The MCBA with solution of air mass balance equation demonstrates an about 1% higher cumulative number of iterations compared to the same method with solution of water mass balance equation. About 30% less iterations are needed to simulate the prescribed time interval using GCBA. While initially GCBA requires more iterations per time step, after several initial time

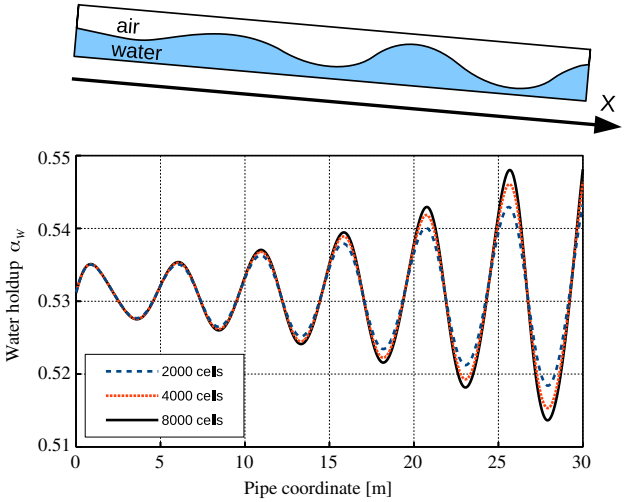

Fig. 4. Water holdup profile along the pipe at $t = 30$ s. Waves are induced by small oscillations of the inlet rates.

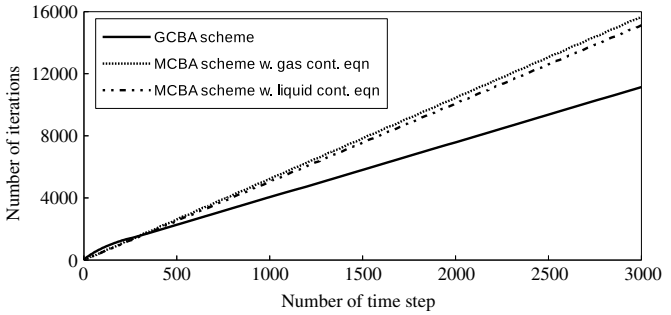

Fig. 5. Cumulative number of non-linear iterations versus time step number for air–water wave flow for GCBA and MCBA numerical schemes.

steps the average number of non-linear iterations starts to decrease and the convergence rate significantly exceeds the one for MCBA.

It should be noted that the difference between the compared schemes depends on the specific case and can substantially exceed these values. For example, for the horizontal pipe with diameter $D = 0.1$ m, inlet velocities $u_G = 20$ m/s, $u_W = 0.7$ m/s and inlet water holdup $\alpha_W = 0.3 + 0.001 \sin(2\pi t)$ for $N = 250$ cells and fixed time step $\tau = 5 \cdot 10^{-4}$ s the cumulative number of iterations differs in about two times if solving water mass balance equation and three times if solving air mass balance equation.

Results for MCBA presented above are obtained for the algorithm without holdups normalization (i.e., when one of mass balance equations was ignored). The scheme with normalization, in terms of equations imbalances convergence criteria, become inapplicable. The relative residuals norm demonstrates the convergence on the scales of 10^{-12}, which is comparable with machine accuracy, but these variables distributions do not satisfy the equations imbalance criteria. While the MCBA scheme that drops one of the mass balance equations provides the linear convergence rate for the equations imbalances, the scheme with normalization provides the linear convergence until some level only, and after that the imbalances stagnate about this point. Numerical experiments demonstrate that even if at the initial time steps the stagnation point is obtained below the limiting point, the imbalance for the mass balance equations will have a strong tendency to increase in time.

5.2. Oil–water segregation

Oil–water segregation is a standard validation case for drift–flux models. The problem considers oil–water segregation in a closed vertical pipe. The mixture with one fluid and two phases corresponds to the graph in Fig. 3(b). The initial state for this problem assumes the top part of the pipe is occupied with water and the bottom part is occupied with oil; the velocities of the phases are set to zero. As the density of the oil is lower than the water density, this state is unstable and the phases start to flow due to the action of gravity forces. At the end of segregation process, the phases change places.

The phase segregation comprises various flow regimes: water with oil droplets, oil with water droplets, layers of oil and water and other. The detailed closures for drift–flux equation (12) covering listed flow regimes are collected in Table B.5.

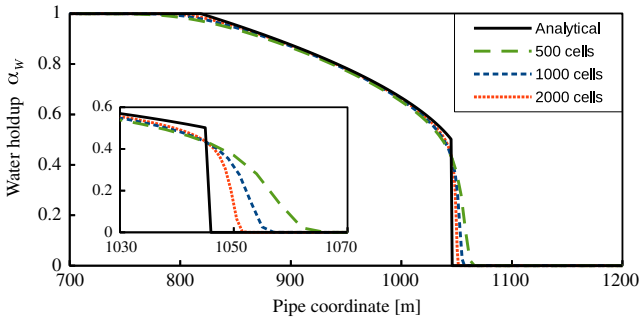

Fig. 6. Water holdup profiles for different computational grids at $t = 1080$ s compared with analytical solution.

Table 3
Grid convergence for the front position ($\alpha_W = 0.01$) in the segregation test case.

Grid	500	1000	2000	Analytical
Front position (m)	1064.2	1056.3	1051.4	1045.2
Front deviation (m)	19	11.1	6.2	–

In the limiting case of incompressible fluids the segregation problem with oil–water closure relations has a self-similar analytical solution as long as the boundary does not impact the flow (see [23]). The profile of water holdup α_W consists of shock wave and rarefaction wave. Shock wave goes down with the front propagation velocity $V_D(0, \beta)/4$ and rarefaction wave goes up with the front propagation velocity $V_D(0, \beta)$ (in the following formula the arguments for the drift velocity are omitted):

$$\alpha_W(x,t) = \begin{cases} 1, & x < L/2 - V_D t; \\ \dfrac{1}{3}\left(1 + \sqrt{1 - 3\dfrac{x - L/2}{V_D t}}\right), & L/2 - V_D t \le x < L/2 + V_D t/4; \\ 0, & x \ge L/2 + V_D t/4. \end{cases} \tag{48}$$

In the current test case, the pipe of diameter $D = 0.1$ m and length $L = 2000$ m is chosen. The phases densities and viscosities are defined in Table 1. Analytical water holdup profile at time step $t = 1080$ s and corresponding numerical simulation profiles for three computational grids are presented in Fig. 6. The deviation of the front position from the analytical solution for different computational grids, demonstrating the grid convergence, is summarized in Table 3. The process of intrusion of the water front into the oil zone and following displacement of the oil phase to the top of the pipe is demonstrated in Fig. 7.

5.3. Stabilization of gas–oil flow

The next problem considers gas–oil flow in a vertical pipe, where gas is presented both in the free phase and in the dissolved form in live oil phase (Fig. 3(c)). The equations of state are based on the black oil model (26). The properties of the phases are specified in Table 1.

We consider a vertical pipe of length $L = 600$ m and diameter $D = 0.1$ m. The inlet condition is specified at the bottom of the pipe. Gas and oil have velocities at the inlet $u_{G0} = 11.63$ m/s, and $u_{O0} = 4.29$ m/s and oil holdup is equal to $\alpha_{O0} = 0.14$. These parameters correspond to the annular flow regime in the pipe [21]. The initial holdups correspond to the prescribed inlet values. The outlet pressure of the mixture changes stepwise from 11 MPa every 400 s by 5 MPa to 1 MPa.

For steady state flow, two-fluid model with gas release can be deduced to the system of equations as follows:

$$\frac{d}{dx}\left(\alpha_O \rho_{O1} u_O\right) = 0, \tag{49}$$

$$\frac{d}{dx}\left(\left(1 - \alpha_O\right) \rho_G u_G + \alpha_O \rho_{O2} u_O\right) = 0, \tag{50}$$

$$\rho_O \alpha_O u_O \frac{du_O}{dx} = -\alpha_O \frac{dp}{dx} - \frac{\Phi_L}{A} - \alpha_O \rho_O g, \tag{51}$$

$$\rho_G \left(1 - \alpha_O\right) u_G \frac{du_G}{dx} = -\left(1 - \alpha_O\right) \frac{dp}{dx} - \frac{\Phi_G}{A} - \left(1 - \alpha_O\right) \rho_G g. \tag{52}$$

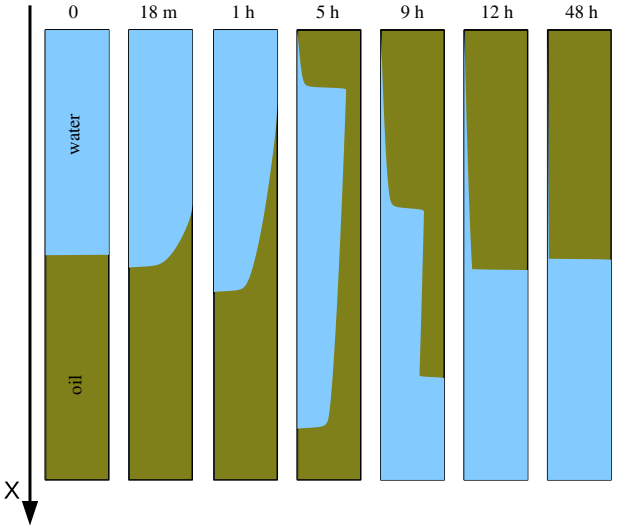

Fig. 7. Evolution of holdups along the pipe during the segregation process.

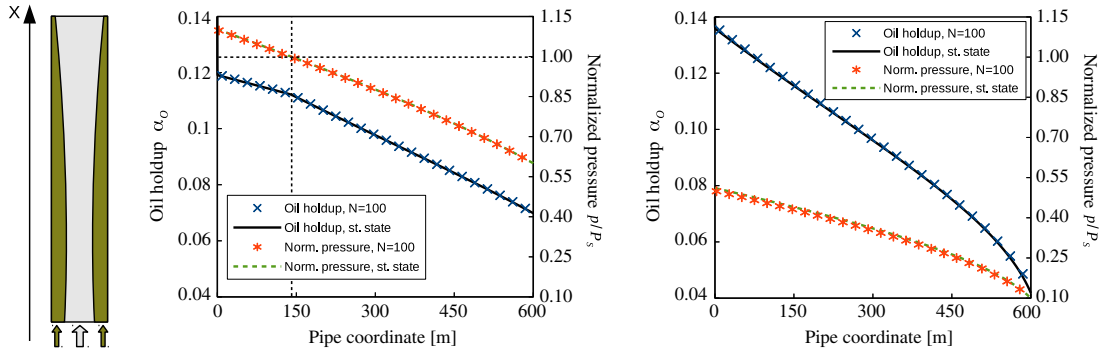

(a) Sketch. (b) $t = 700$ s, $P_{out} = 6$ MPa. (c) $t = 1100$ s, $P_{out} = 1$ MPa.

Fig. 8. Schematic of the flow in the vertical pipe with gas release. Liquid holdup and pressure profiles.

In between pressure drops, the flow stabilizes then it is described with (49)–(52). The integration of the problem (49)–(52) provides the reference solutions. Fig. 8 shows the profiles of holdup and pressure for the two time steps. First flow stabilization takes place at $t = 700$ s when the outlet pressure is 6 MPa (Fig. 8(b)). There is a zone with gas release at the top of the pipe is obtained above the bend of the holdup profile at 140 m. The mass exchange due to gas release increases gas holdup along the pipe. The bend of holdup corresponds to the bubble point where gas release originates. The profiles on Fig. 8(c) correspond to the flow stabilization after the second pressure drop. Pressure at the bottom of the pipe is below 5.2 MPa, thus the gas release occurs along the whole pipe. The liquid film on the pipe walls shrinks to the top of the pipe due to the acceleration of the gas phase and the action of interphase friction forces. Presented results demonstrate a good match between the reference steady solutions and the numerical solution of the transient model.

The corrections for the mass exchange term in the GCBA scheme, discussed in Section 4.3, are necessary to obtain numerical solution for this test case. Attempts to simulate the case without corrections for the mass exchange term failed due to the non-linear iterations divergence, regardless the integration time step and the numerical method used.

5.4. Five-phase mixture flow in a wellbore

Finally, let us consider the flow of mixture with 5 phases (Fig. 3(d)) in the deviated wellbore. The oil–water mixture comprises compressible phases with different reference densities: $\rho_{Phase1} = 700$ kg/m^3, $\rho_{Phase2} = 750$ kg/m^3, $\rho_{Phase3} = 800$ kg/m^3, $\rho_{Phase4} = 1000$ kg/m^3, $\rho_{Phase5} = 1100$ kg/m^3. Phases 1, 2, and 3 are oil-based, phases 4 and 5 are water-based. The slip between the oil-based phases and the mixture of the water phases is specified according to the drift–flux relations (12). There is no slip between the water-based phases (see, Fig. 3(d)). The oil–water drift–flux parameters used in the simulations are collected in Table B.5.

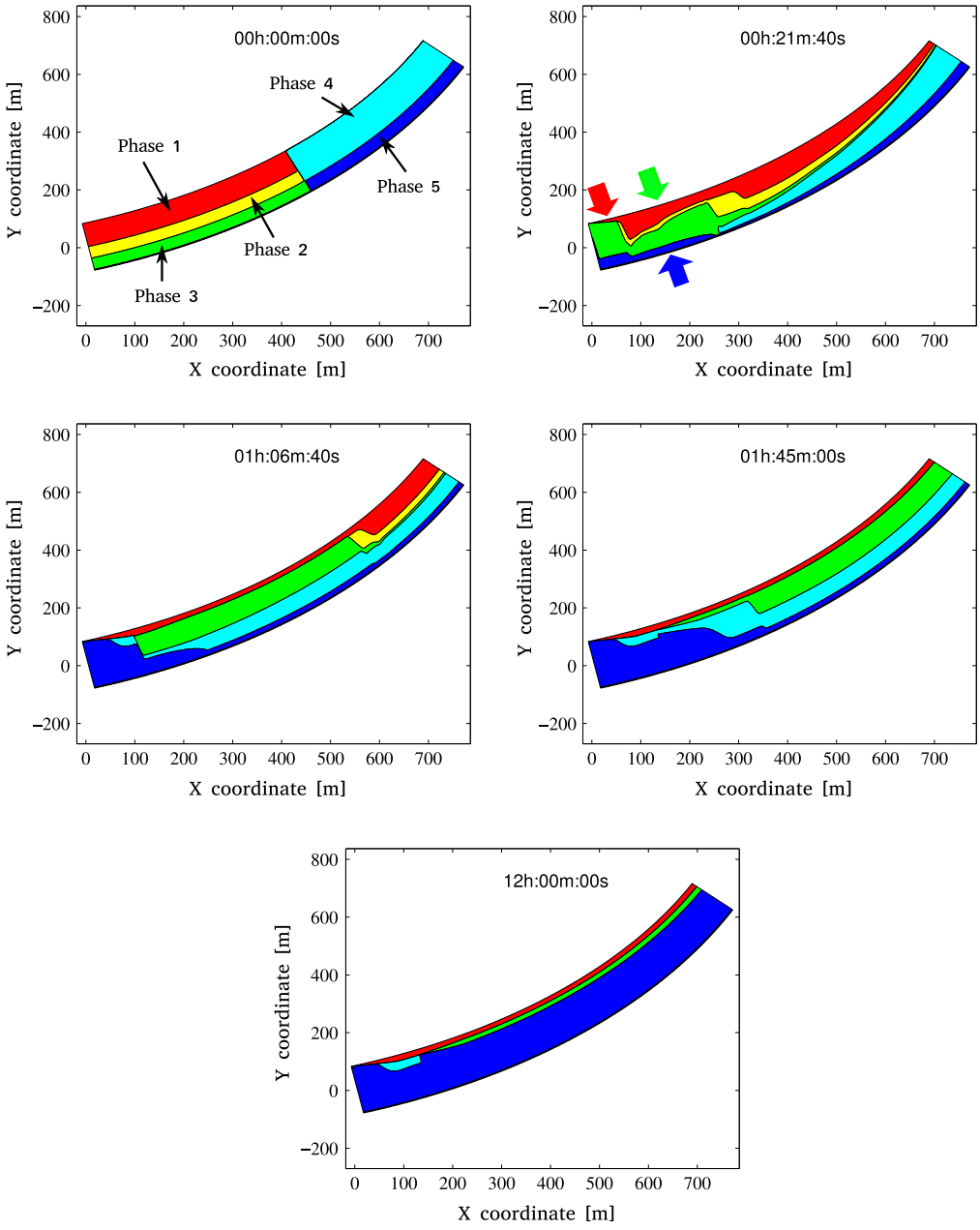

Fig. 9. Five-phase flow in a deviated wellbore.

The wellbore has a length of $L = 1000$ m and a diameter of $D = 0.1$ m. The wellbore inclination changes linearly from $\pi/9$ to $\pi/4$. The bottom portion of the wellbore is filled with oil phases $\alpha_{Phase1} = 0.5$, $\alpha_{Phase2} = 0.25$, $\alpha_{Phase3} = 0.25$. The top portion of the wellbore is filled with water phases $\alpha_{Phase4} = 0.75$, $\alpha_{Phase5} = 0.25$. The wellbore is closed at the bottom. The top part is open and exposed to the constant pressure 100 MPa. Initially the pressure is hydrostatic. There are steady inflows of phases 1, 3, and 5 in the range 0–100 m and 150–250 m, equal to 0.003 kg/(m s). They imitate the inflows from the reservoir at the well completion parts, see Fig. 9. The wellbore diameter in Fig. 9 is magnified, holdups are stacked on top of each other regardless the flow structure.

Initial distribution of the phases is shown in Fig. 9. The flow has two stages: segregation and stabilization. During the segregation the heavy water phases sink to the bottom. Phases 4 and 5 fully displace the oil-based phases 2 and 3 from the bottom of the pipe. After 1 hour the flow tends to the steady state. The light phases are ejected from the well by the heavy phases. In Fig. 9 one can see that after 2 h the heavy phase 5 occupied the wellbore bottom end and the wellbore contains the phases flowing from the reservoir. This simulation evaluates a number of values important for well start up, such as time of a phase appearance to the top, time of complete cleanup of a phase, and time of flow stabilization.

6. Conclusions

A general multiphase pipe flow model, based on the combination of multi-fluid and drift–flux approaches, is proposed. The model allows to simulate the flows with arbitrary number of phases including the mass exchange phenomena. A graph interpretation for the proposed model is discussed. It is shown that the principal information about the mixture can be stored in a tree-like graph. Different levels of the graph correspond to immiscible phases and interpenetrating components within each fluid. The top level of the graph represents the mixture. The fluids located at the second level are described by the full momentum conservation equations, while the components occupying lower levels are described by the drift–flux model based on the assumption of a non-inertial interphase slip. The edges of the graph represent the relations between the mixture, fluids, components, and phases.

The SIMPLE numerical algorithms are adopted to handle various multiphase models. The algorithms handle a graph reflecting a mixture structure. The generalizations for both mass and geometry conservation based methods are discussed in the paper. Additional GCBA-specific corrections to model an equilibrium gas release are proposed. The efficiency of the methods based on mass and geometry conservation principles is investigated. The GCBA methods provide better convergence rates compared to MCBA ones for the two-fluid wave flow examined. Ignorance of additional corrections to model gas release may lead to scheme divergence. These observations make the GCBA schemes preferable in our simulations.

The proposed mathematical model with graph representation and corresponding generalization for numerical methods provides a flexible framework to model the flows with mixtures of arbitrary complexity. The research code implemented deals with the graph representation while the mathematical model is automatically adjusted on the information provided by the graph. Various examples of mathematical models and corresponding graphs are demonstrated in the paper. The further plans on this study should cover the extension of this model on mass transfer between the dispersed and continuous phases and improvements on the stability of numerical schemes for slug flow simulations.

The multiphase flow simulators are in a big demand by the industry. The specific simplified 1D branch of the simulators is in favour due to acceptable CPU performance and rich experimental base of measurements. Our model proposes the generalization of the one-dimensional approach. The graph construction can be a first step on the understanding of the mixture structure and multiphase flow modelling.

Acknowledgements

The authors are grateful to Bertrand Theuveny, Pavel Spesivtsev and Konstantin Sinkov for insights into practical aspects of oil and gas wellbore flows and discussions on the drift–flux model implementation.

Appendix A. Well-posed hyperbolic model

For two fluids, one can get a well-posed hyperbolic model introducing into momentum equation either a virtual mass term [16,26] or a term with interfacial pressure [6,7,41]. In [7], the authors have compared virtual masses and interfacial pressure term, both affect steady state flows negligibly and vary eigenvalues in the acceptable range. The virtual mass force concept is well-established for dispersed continua when one can average virtual mass force of particles (or bubbles, or droplets). The main focus of the current paper, however, is on modelling flows with continuous fluids (stratified or annular flows) and the physical analogy of virtual mass forces is not so evident here. Thus, any significant advantage for the virtual mass force against the interfacial pressure term or vice versa is unclear. There is a wide discussion in the literature on the hyperbolicity of 1D multi-fluid models (see, [6,7,42,43]), but there is no general conclusion about the benefits of one approach over the other one.

The interfacial pressure term is used in our study to preserve hyperbolicity. Then, the incompressible two-fluid model has the eigenvalues as follows:

$$\lambda_{1,2} = \infty, \tag{A.1}$$

$$\lambda_{3,4} = \frac{\alpha_L \rho_G u_G + \alpha_G \rho_L u_L}{\alpha_G \rho_L + \alpha_L \rho_G} \pm \sqrt{\frac{A_H - A_U + P_I}{\alpha_G \rho_L + \alpha_L \rho_G}}, \tag{A.2}$$

$$A_H = \alpha_L \alpha_G \left(\rho_L - \rho_G\right) g \frac{dH_L}{d\alpha_L} \cos\beta, \tag{A.3}$$

$$A_U = \frac{\alpha_L \alpha_G \rho_L \rho_G (u_G - u_L)^2}{\alpha_G \rho_L + \alpha_L \rho_G}. \tag{A.4}$$

The minimum interfacial pressure to preserve hyperbolicity for the two incompressible fluids is:

$$P_I = A_U. \tag{A.5}$$

Table B.4
Closures for friction in gas–liquid flow.

Property	Closure	Flow regime
Pipe diameter, D	$2\sqrt{A/\pi}$	
Gas friction coefficient, f_G	$\frac{16}{Re_G}$	S, L [45]
	$\frac{0.046}{Re_G^{0.2}}$	S, T [45]
	0	A
Liquid friction coefficient, f_L	$\frac{24}{Re_L}$	S, L [27]
	$\frac{0.0262}{(\alpha_L Re_L)^{0.139}}$	S, T [27]
	$\frac{16}{Re_L}$	A, L [45]
	$\frac{0.046}{Re_L^{0.2}}$	A, T [45]
Interfacial friction coefficient, f_I	$\frac{16}{Re_I}$	S, L [45]
	$\frac{0.046}{Re_I^{0.2}}$	S, T [45]
	$0.005\left(1+300\frac{\delta}{D}\right)$	A [46]
Reynolds number for gas, Re_G	$\frac{\rho_G\lvert u_G\rvert}{\mu_G}\frac{4\alpha_G A}{S_G+S_I}$	S
Reynolds number for liquid, Re_L	$\frac{\rho_L\lvert u_L\rvert\alpha_L D}{\mu_L}$	All
Reynolds number for relative velocity, Re_I	$\frac{\rho_G\lvert u_G-u_L\rvert}{\mu_G}\frac{4\alpha_G A}{S_G+S_I}$	S
Gas contact with wall, S_G	$(2\pi-\gamma)\frac{D}{2}$	All
Liquid contact with wall, S_L	$\gamma\frac{D}{2}$	All
Gas–liquid contact, S_I	$D\sin\frac{\gamma}{2}$	S
	$\pi D\sqrt{\alpha_G}$	A
Contact angle, γ	$\gamma-\sin\gamma=2\pi\alpha_L$	S
	2π	A
Liquid film thickness, δ	0	S
	$\frac{D}{2}\left(1-\sqrt{\alpha_G}\right)$	A
Height of stratified liquid layer, H_L	$\frac{D}{2}\left(1-\cos\frac{\gamma}{2}\right)$	S
	0	A

A—annular flow, S—stratified flow, L—laminar regime, T—turbulent regime.

This condition proposes the regularization in explicit and unconditional form. The case of two compressible fluids can be regularized when multiplying A_U by scalar $\theta > 1.2$ (see [7] for more details):

$$P_I = \theta A_U. \tag{A.6}$$

The hyperbolicity remains an open question for the multi-fluid model. If number of fluids exceeds two, the hyperbolicity domain has to be investigated in the space of many parameters. The investigation then involves solution of polynomial equations of high degree [44].

Appendix B. Friction closures for multiphase model

In the case of two-fluid gas–liquid flows, the friction terms in momentum equation have a form (10)–(11). According to [9], different friction closures are required for stratified and annular flow regimes. The slug flow regime can be modelled directly as a result of instability of the stratified flow at the interface (slug capturing). Friction coefficients f_{km} for these flow regimes are collected in Table B.4, here the liquid density is assumed greater than the gas density. Stability theory for stratified flow provides the criteria of transition between the stratified and annular flows, which has a good correspondence with experimental data [45,20]:

$$|u_G - u_L| > \sqrt{(\rho_L\alpha_G + \rho_G\alpha_L)\,\frac{\rho_L-\rho_G}{\rho_L\rho_G}g\cos\beta\frac{dH_L}{d\alpha_L}}, \tag{B.1}$$

$$\alpha_L < 0.5. \tag{B.2}$$

The drift–flux correlations for the profile parameter and the drift velocity, valid for inclined and vertical pipes, were proposed in [31]. The further extension on the near-horizontal pipes starting from 2° was suggested in [4]. The corresponding oil–water correlations [31], used in the simulations, are gathered in Table B.5.

Table B.5
Closures for oil–water drift–flux model.

Property	Closure
Inclination factor, $m(\beta)$	$(\sin\beta)^{0.5}(1+\cos\beta)^2$
Drift–flux parameter, b	$\frac{\alpha_O}{\alpha_O+\alpha_W}$
Profile parameter, $C_0(b)$	$\begin{cases} A', & b < B_1'; \\ A' + (1-A')\dfrac{b-B_1'}{B_2'-B_1'}, & B_1' \le b \le B_2'; \\ 1, & b > B_2'. \end{cases}$ $A' = 1.2, B_1' = 0.4, B_2' = 0.7$
Small oil droplet rise velocity, V_C	$\sqrt[4]{\frac{\sigma_{OW} g(\rho_W-\rho_O)}{\rho_W^2}}$
Drift velocity, $V_D(b,\beta)$	$1.53m(\beta)(1-b)^2V_C$

σ_{OW} is an oil–water surface tension coefficient. It varies within range 10–100 mN/m. In the validation cases, it is set equal to 74 mN/m.

Appendix C. Mass conservation-based approach for graph-based mathematical model

Based on the same principles as generalization for GCBA methods, the generalization for MCBA methods family could be done. Assume the solution for nth time step is known and the next time step should be found. The solution for the next time step begins with obtaining preliminary velocity fields u_k^* by solving momentum equations (2) for every fluid vertex of the graph. After that, the overall mass balance equation is formulated from the fluids mass balance equations to enforce the global mass conservation [39]. This equation is defined as a linear combination of fluids mass balance equations, where the weights are inversely proportional to some reference densities of the fluids:

$$\sum_{k=1}^{K} \frac{1}{\rho_k^{ref}} \left(\frac{\partial \alpha_k \rho_k A}{\partial t} + \frac{\partial \alpha_k \rho_k u_k A}{\partial x} \right) = \sum_{k=1}^{K} \frac{1}{\rho_k^{ref}} J_k. \tag{C.1}$$

The residual for this discretized equation characterizes the overall mass imbalance. If residual obtained with preliminary velocity fields u_k^* is higher than some prescribed limiting value, the velocities will be corrected.

Representing the pressure, densities and velocities in the form of preliminary values and its corrections (31) one can obtain the velocity correction as a function of pressure correction (32). Using velocity corrections (32) and neglecting higher order terms in (C.1), the discrete pressure correction equation can be obtained. After solution of Eq. (C.1), the velocities of the fluids and the pressure can be corrected.

Densities of the phases are defined from the equations of state (7) with the new pressure field and restored for all other components and fluids moving upward over the graph using preliminary holdups. Velocities for all the components and phases with new densities can be restored, starting from the fluids and moving down over the graph. Having velocities and densities, one can find the holdups for the phases from the mass balance equations and restore the new values for the components and fluids.

The non-trivial question for MCBA schemes is the solution of mass balance equations to define holdups. Generally speaking, holdups for the fluids, phases, and components should satisfy N mass balance equations for terminal vertices, L holdup constraints (3), and the holdup constraint for the mixture α_M (6) (i.e., $S+1$ equations for S variables). On the other hand, linear combination of mass balance equations was already used to construct the overall mass balance equation. Mainly, the following two methodologies to resolve this issue are suggested in the literature:

(i) to drop one of the mass balance equations and use the holdup constraint to obtain the corresponding phase volume fraction (e.g. [8]);
(ii) to solve all the mass balance equations, and then to normalize all the holdups in order to preserve the holdup constraint (6) (e.g. [47]).

Both methods, however, have some disadvantages. The first method provides a degree of freedom as to which of equations should be ignored when solving for holdups. Moreover, the choice of equation to be dropped may vary along the pipe depending on the presence of the specific phase in the grid cell. The second option assumes the forced modification for the holdup distributions, and there is no guarantee the results of this normalization would satisfy the mass balance equations. A detailed discussion on different approaches for solution of mass balance equations can be found in [48].

To conclude, the mass conservation-based algorithm to obtain solution at the next time step consists of eight steps:

1. Find preliminary velocity fields, u_k^*, for the fluid phases.
2. Check for overall mass conservation equation imbalance; if the imbalance is lower than the limiting value, then go to 6, otherwise go to 3.
3. Solve the pressure correction equation; find pressure correction, p'.
4. Correct pressure and fluids velocities.
5. Update the density fields with new pressure distribution using equations of state.

6. Find velocities for components and phases.
7. Find holdups for the phases; restore values for all components and fluids.
8. Check the convergence criteria; continue non-linear iterations from 1 if convergence is not reached.

References

[1] M. Ishii, T. Hibiki, Thermo-Fluid Dynamics of Two-Phase Flow, second ed., Springer-Verlag, New York, 2011.
[2] D.A. Drew, Mathematical modeling of two-phase flow, Annu. Rev. Fluid Mech. 15 (1) (1983) 261–291.
[3] N. Zuber, J.A. Findlay, Average volumetric concentration in two-phase flow systems, J. Heat Transfer 87 (1965) 453–468.
[4] H. Shi, J.A. Holmes, L.J. Durlofsky, K. Aziz, L. Diaz, B. Alkaya, G. Oddie, Drift–flux modeling of two-phase flow in wellbores, SPE J. 10 (1) (2005) 24–33. SPE-84228-PA.
[5] S.T. Munkejord, S. Evje, T. Fltten, The multi-stage centred-scheme approach applied to a drift–flux two-phase flow model, Internat. J. Numer. Methods Fluids 52 (6) (2006) 679–705.
[6] D. Bestion, The physical closure laws in the CATHARE code, Nucl. Eng. Des. 124 (3) (1990) 229–245.
[7] I. Tiselj, S. Petelin, Modelling of two-phase flow with second-order accurate scheme, J. Comput. Phys. 136 (2) (1997) 503–521.
[8] R. Issa, M. Kempf, Simulation of slug flow in horizontal and nearly horizontal pipes with the two-fluid model, Int. J. Multiph. Flow 29 (1) (2003) 69–95.
[9] M. Bonizzi, P. Andreussi, S. Banerjee, Flow regime independent, high resolution multi-field modelling of near-horizontal gas–liquid flows in pipelines, Int. J. Multiph. Flow 35 (1) (2009) 34–46.
[10] B. Krasnopolsky, A. Starostin, A. Osiptsov, Multi-fluid pipe flow model for analysis of wellbore dynamics, AIP Conf. Proc. 1479 (1) (2012) 99–103.
[11] A. Osiptsov, K. Sinkov, P. Spesivtsev, Justification of the drift–flux model for two-phase flow in a circular pipe, Fluid Dyn. 49 (5) (2014) 614–626.
[12] M.E. Abou-El-Hassan, Correlations for bubble rise in gas–liquid systems, in: Encyclopedia of Fluid Mechanics: Gas-Liquid Flows, vol. 3, GULF, 1986.
[13] A. Lapin, A. Lbbert, Numerical simulation of the dynamics of two-phase gas–liquid flows in bubble columns, Chem. Eng. Sci. 49 (21) (1994) 3661–3674.
[14] O. Bratland, Pipe flow 2: Multiphase flow assurance, 2009.
[15] J. Choi, E. Pereyra, C. Sarica, C. Park, J.M. Kang, An efficient drift–flux closure relationship to estimate liquid holdups of gas–liquid two-phase flow in pipes, Energies 5 (12) (2012) 5294–5306.
[16] I. Toumi, A. Kumbaro, An approximate linearized Riemann solver for a two-fluid model, J. Comput. Phys. 124 (2) (1996) 286–300.
[17] K. Bendiksen, D. Maines, R. Moe, S. Nuland, The dynamic two-fluid model OLGA: Theory and application, SPE Prod. Eng. 6 (2) (1991) 171–180. SPE-19451-PA.
[18] M. Bonizzi, R. Issa, On the simulation of three-phase slug flow in nearly horizontal pipes using the multi-fluid model, Int. J. Multiph. Flow 29 (11) (2003) 1719–1747.
[19] V. Alipchenkov, R. Nigmatulin, S. Soloviev, O. Stonik, L. Zaichik, Y. Zeigarnik, A three-fluid model of two-phase dispersed-annular flow, Int. J. Heat Mass Transfer 47 (24) (2004) 5323–5338.
[20] O. Shoham, Flow pattern transition and characterization in gas–liquid two phase flow in inclined pipes (Ph.D. thesis), Tel-Aviv Univ, Ramat-Aviv, Israel, 1982.
[21] D. Barnea, Y. Taitel, Interfacial and structural stability of separated flow, in: Annual Reviews in Multiphase Flow, Pergamon Press Ltd., 1994, pp. 387–414.
[22] M. Bonizzi, Transient one-dimensional modelling of multi-phase slug flows (Ph.D. thesis), Imperial College, University of London, 2003.
[23] P. Spesivtsev, K. Sinkov, A. Osiptsov, Modeling of wellbore phase segregation during shut-in using the drift–flux model, in: Proceedings of 8-th International Conference on Multiphase Flow, 2013.
[24] M. Bonizzi, R. Issa, A model for simulating gas bubble entrainment in two-phase horizontal slug flow, Int. J. Multiph. Flow 29 (11) (2003) 1685–1717.
[25] OLGA 7 User Manual, 2014.
[26] S. Pudasaini, A general two-phase debris flow model, J. Geophys. Res. 117 (2012) 551–560.
[27] P. Spedding, N. Hand, Prediction in stratified gas–liquid co-current flow in horizontal pipelines, Int. J. Heat Mass Transfer 40 (8) (1997) 1923–1935.
[28] D. Bestion, The phase appearance and disappearance in the CATHARE code, in: Trends in Numerical and Physical Modeling for Industrial Multiphase Flows, 2000.
[29] F. Cordier, P. Degond, A. Kumbaro, Phase appearance or disappearance in two-phase flows, J. Sci. Comput. 58 (1) (2013) 115–148.
[30] H. Paillere, C. Corre, J.G. Cascales, On the extension of the AUSM+ scheme to compressible two-fluid models, Comput. & Fluids 32 (6) (2003) 891–916.
[31] A. Hasan, C. Kabir, A simplified model for oil/water flow in vertical and deviated wellbores, SPE Prod. Facil. 14 (1) (1999) 56–62. SPE-54131-PA.
[32] J.A. Trangenstein, J.B. Bell, Mathematical structure of the black-oil model for petroleum reservoir simulation, SIAM J. Appl. Math. 49 (3) (1989) 749–783.
[33] Q. Li, S. Fu, A gas-kinetic BGK scheme for gas-water flow, Comput. Math. Appl. 61 (12) (2011) 3639–3652. Mesoscopic Methods for Engineering and Science - Proceedings of ICMMES-09 Mesoscopic Methods for Engineering and Science.
[34] R. Moe, K.H. Bendiksen, Transient simulation of 2D and 3D stratified and intermittent two-phase flows. Part I: Theory, Internat. J. Numer. Methods Fluids 16 (6) (1993) 461–487.
[35] S. Patankar, Numerical Heat Transfer and Fluid Flow, CRC Press, 1980.
[36] F. Moukalled, M. Darwish, A unified formulation of the segregated class of algorithms for fluid flow at all speeds, Numer. Heat Transfer B 37 (1) (2000) 103–139.
[37] W. Rivard, M. Torrey, Kfix: A program for transient two dimensional two fluid flow, Tech. Rep. LA-NUREG-6623, 1978.
[38] D. Spalding, Numerical computation of multi-phase fluid flow and heat transfer, in: C. Taylor, K. Morgan (Eds.), Recent Advances in Numerical Methods in Fluid, Vol. 1, Pineridge Press, 1980, pp. 139–167.
[39] F. Moukalled, M. Darwish, Pressure-based algorithms for multifluid flow at all speeds — part I: Mass conservation formulation, Numer. Heat Transfer B 45 (6) (2004) 495–522.
[40] F. Moukalled, M. Darwish, Pressure-based algorithms for multifluid flow at all speeds — part II: Geometric conservation formulation, Numer. Heat Transfer B 45 (6) (2004) 523–540.
[41] J. Stuhmiller, The influence of interfacial pressure forces on the character of two-phase flow model equations, Int. J. Multiph. Flow 3 (1977) 551–560.
[42] C. Omgba-Essama, Numerical modelling of transient gas–liquid flows (application to stratified & slug flow regimes) (Ph.D. thesis), Cranfield University, 2004.
[43] T.N. Dinh, R.R. Nourgaliev, T.G. Theofanous, Understanding of the ill-posed two-fluid model, in: Proceedings of the Tenth International Topical Meeting on Nuclear Reactor Thermal Hydraulics, 2003.
[44] V. Zhibaedov, N. Lebedeva, A. Osiptsov, K. Sin'kov, On the hyperbolicity of one-dimensional models for transient two-phase flow in a pipeline, Fluid Dyn. (1) (2016) 56–69.
[45] Y. Taitel, A.E. Dukler, A model for predicting flow regime transitions in horizontal and near horizontal gas–liquid flow, AIChE J. 22 (1) (1976) 47–55.
[46] Wallis, One-Dimensional Two-Phase Flow, McGraw-Hill, New York, 1969.
[47] D. Spalding, The numerical computation of multi-phase flows, Tech. Rep. Report CFD/85/7, Imperial College London, 1985.
[48] H. Rusche, Computational fluid dynamics of dispersed two-phase flows at high phase fractions (Ph.D. thesis), Imperial College of Science, Technology & Medicine, 2002.